Size-dependent melting properties of tin nanoparticles

Hongjin Jiang [a], Kyoung-sik Moon [a], Hai Dong [a], Fay Hua [b], C.P. Wong [a,*]

[a] School of Materials Science and Engineering, School of Chemistry and Biochemistry, Georgia Institute of Technology, Love Building, 771 Ferst Drive, Atlanta, GA 30332, United States
[b] Materials Technology Operation, Intel Corporation, 3065 Bowers Avenue, Santa Clara, CA 95054, United States

Abstract

Tin nanoparticles with various sizes were synthesized by the chemical reduction method and their thermal properties were first studied by differential scanning calorimetry. Both particle size dependent melting temperature and latent heat of fusion have been observed. The experimental results in this study showed reasonable agreement with the thermodynamics model.
© 2006 Elsevier B.V. All rights reserved.

1. Introduction

In electronic devices, tin and some of its alloys are being used as interconnect materials in on-chip and off-chip applications. Due to their high melting point (220–240 °C), a high reflow temperature will be needed in the electronics manufacturing process. This high process temperature in electronics assembly has adverse effects not only on energy consumption, but also on substrate warpage, thermal stress and popcorn cracking in molding compounds, resulting in poor reliability of the devices. Therefore studies on lowering processing temperature of Sn are being paid attention.

The melting point of substances can be dramatically decreased when their size is reduced to nanometer size [1–11]. This is due to the high surface area to volume ratio for small particles, which as a consequence of the higher surface energy substantially affects the interior 'bulk' properties of the material, resulting in a decrease of the melting point. The outer surface of the nanoparticles plays a relevant role in the melting depression.

Till now, transmission electron microscopy (TEM) and nanocalorimeter have been used to study the melting behavior of single Sn nanoparticle or cluster. At the melting point, the diffraction pattern of the crystal structure in TEM exhibited the order–disorder transition [12]. However, unlike calorimeters, TEM cannot measure the latent heat of fusion (ΔH_m), which is very useful to understand the thermodynamics of a finite material system. Lai et al. investigated the melting process of supported Sn clusters by nanocalorimeter [2] and found the melting point depended nonlinearly on the inverse of the cluster radius R, which was in contrast to the traditional description of the melting behavior of small particles. They first reported a particle-size-dependent reduction of ΔH_m for Sn nanoparticles. Bachels et al. studied the melting behavior of isolated Sn nanoparticles or clusters by nanocalorimeter as well [3]. The melting point of the investigated Sn clusters was found to be lowered by 125 K and the latent heat of fusion per atom was reduced by 35% compared to bulk Sn. However, for both the TEM and nanocalorimetric measurements, the single element of Sn nanoparticle or the cluster was synthesized by the deposition method inside the measurement equipments in order to prevent the particles from oxidation. Although this synthesis method was sufficiently sophisticated for the pure observation, the real world synthesis and the characterization possess more experimental parameters to consider such as oxidation during moving samples and differences in melting/wetting behavior on different substrate materials.

* Corresponding author. Fax: +1 404 894 9140.
E-mail address: cp.wong@mse.gatech.edu (C.P. Wong).

In this study, Sn nanoparticles were synthesized by chemical reduction method. This method is more suitable for the Sn nanoparticle synthesis because the chemical reduction can use a low temperature, resulting in a better control of thermal oxidation of Sn nanoparticles. During the synthesis process, surfactants were used to protect the Sn nanoparticle from oxidation. The conventional differential scanning calorimetry (DSC) was first used to investigate the melting behavior of the as-synthesized different sized Sn nanoparticle powders. Both the size dependency of the melting point and the latent heat of fusion are presented.

2. Experimental

2.1. Materials

Tin (II) acetate, sodium borohydride, and anhydrous methanol were used as precursors, reducing agents and solvents respectively. These chemicals were all purchased from Aldrich and used without further purification.

2.2. Synthesis

A certain amount of tin (II) acetate and surfactants were mixed into a 60 ml anhydrous methanol solution. The solution was stirred and nitrogen purged for 2 h. Then, 0.1 g sodium borohydride was added to the solution and the reaction continued for another 2 h at room temperature.

2.3. Characterization

Transmission electron microscopy (TEM, JEOL 100C TEM) was used to observe the morphologies of the synthesized nanoparticles. TEM specimens were prepared by dispersing a few drops of the Sn nanoparticle solution onto a carbon film supported by copper grids. X-ray diffraction (XRD, PW 1800) and high resolution transmission electron microscopy (HRTEM, Hitachi 2000K TEM) were used to

study the crystal structure of Sn nanoparticles. A thermogravimetric analyzer (TGA, 2050 from Thermal Advantages Inc.) was used to investigate the thermal degradation of the surfactants anchoring on the Sn nanoparticle surface. The melting point of the Sn nanoparticles was determined by a differential scanning calorimeter (DSC, TA Instruments, model 2970). A sample of about 10 mg was hermetically sealed into an aluminum pan and placed in the DSC cell under nitrogen purge. Dynamic scans were made on the samples at a heating rate of 5 °C/min, from room temperature to 250 °C.

3. Results and discussion

Fig. 1a shows the TEM and inserted HRTEM images of Sn nanoparticles synthesized by using 2.1×10^{-4} mol tin (II) acetate as a precursor in the presence of 0.045 mol surfactants. The average particle size calculated from the TEM picture was around 61 nm and the obvious lattice fringes in HRTEM image implies the crystalline structure. The interplanar spacing was about 0.29 nm which corresponds to the orientation of (2 0 0) atomic planes of the tetragonal structure of Sn. In the XRD pattern (Fig. 1b), all the peaks can be indexed to a tetragonal cell of Sn with $a = 0.582$ and $c = 0.317$ nm. The relative intensity of the peaks was consistent with that of the Sn nanoparticles reported elsewhere [13]. No obvious peaks at 20.6°, 33.8° and 51.8° were found, which match the crystal planes of SnO_2: (1 0 0), (1 0 1) and (2 1 1) [14]. However, the obvious oxidation peaks of SnO_2 were observed from the XRD pattern of the Sn nanoparticles without surfactants. The XRD and HRTEM results showed that the Sn nanoparticles synthesized with surfactants in this study were nearly oxide free.

Fig. 2a shows the TGA curve of the as-synthesized Sn nanoparticles. The weight loss at below 275 °C may be due to the evaporation of absorbed moisture and the decomposition of the surfactants. Above 275 °C, the weight gain was observed. This may be attributed to ther-
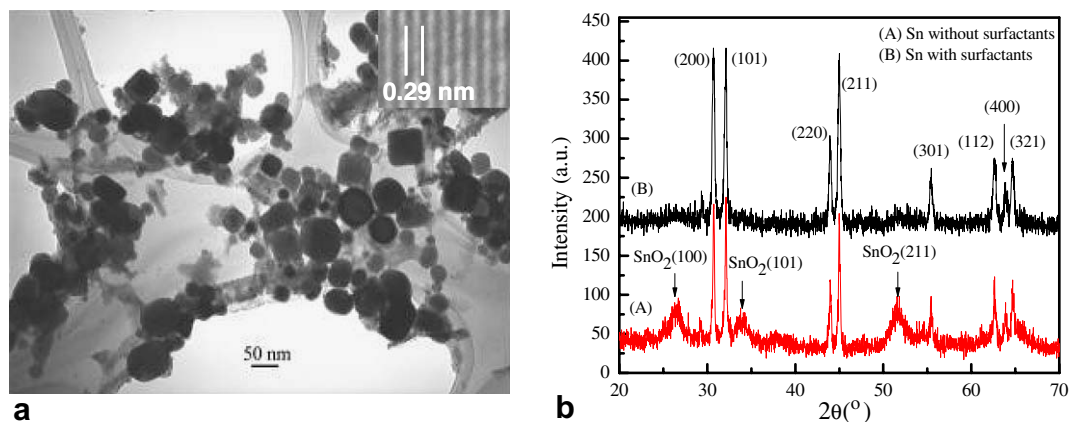
Fig. 1. (a) TEM, inserted HRTEM images and (b) XRD of Sn nanoparticles which were synthesized by using 2.1×10^{-4} mol tin (II) acetate as a precursor in the presence of 0.045 mol surfactants.
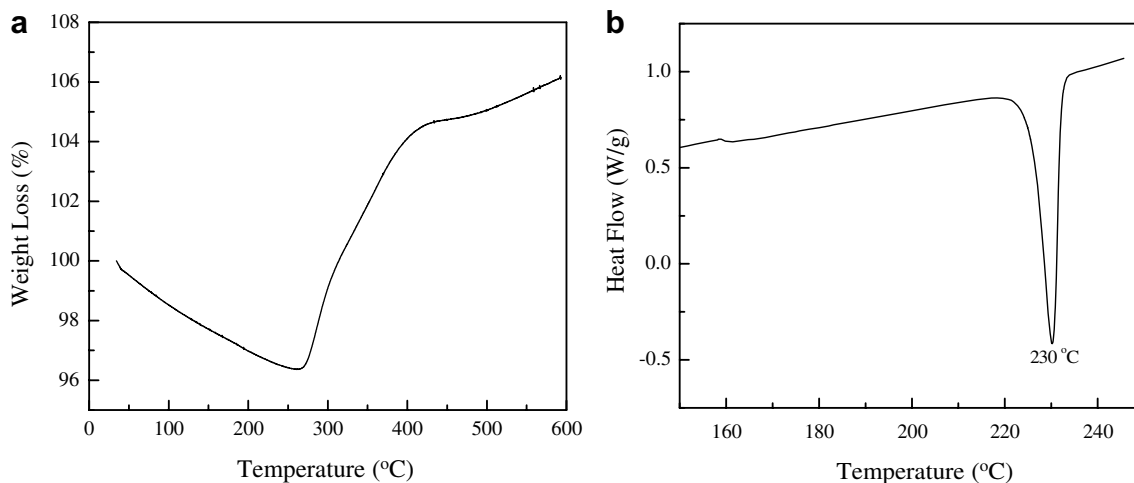
Fig. 2. TGA (a) and DSC (b) curves of the as-synthesized Sn nanoparticles.

mal oxidation of the pure Sn nanoparticles. The TGA results showed that the Sn nanoparticles were covered with the surfactants by ∼4 wt% to the particle weight. And these surfactants can protect the Sn nanoparticles from oxidation. Fig. 2b shows the thermal profiles of the as-synthesized Sn nanoparticles obtained from DSC where the melting point (T_m) was observed at 230 °C. Compared to the T_m of micron sized Sn particles, the Sn nanoparticles exhibited the T_m depression by 2–3 °C.

The oxide-free Sn nanoparticles were obtained by using the different molar ratios between a precursor and a surfactant. Thus, different sized Sn nanoparticles can be obtained.

Fig. 3a,b shows the TEM image and DSC profile of the Sn nanoparticles which were synthesized by using 4.2×10^{-4} mol tin (II) acetate as a precursor in the presence of 0.045 mol surfactants. The average particle size was around 52 nm. The melting point of the Sn nanoparticles was around 228.0 °C, which was 4 °C lower than that of micron sized Sn particles. Fig. 3c,d shows the TEM image and DSC profile of the Sn nanoparticles which were synthesized by using 1.1×10^{-3} mol tin (II) acetate as a precursor in the presence of 0.045 mol surfactants. The average particle size was around 85 nm. The melting point of the as-synthesized Sn nanopartiles was 231.8 °C, which was still lower than the melting point of micron sized Sn particles. The TEM image of Sn nanoparticles which were synthesized by using 1.75×10^{-4} mol tin (II) acetate as a precursor in the presence of 0.045 mol surfactants is shown in Fig. 3e. The average particle size was around 26 nm. The melting point of these particles was around 214.9 °C, which was 17.7 °C lower than that of micron sized Sn particles. The melting transition of this sample took place over a temperature range of about 60 °C, which was much wider than the other three samples. This phenomenon can be attributed to a broadening of the phase transition due to the finite size effect [15] and wide size distribution of the Sn nanoparticles. Schmidt et al. also found a melting tem-

perature range of 60 K for cluster size with the number of atoms between 70 and 200 [7].

From Table 1, it can be seen that the larger molar ratios between the surfactants and the precursors were used, the smaller the particle size was. This is because a larger amount of surfactants can restrict the growth of Sn nanoparticles. The surfactant molecules coordinate with the nanoclusters, resulting in the capping effect to restrict the particle growth. This was also found by Pal et al. on their gold nanoparticle synthesis that increasing the concentrations of surfactants would limit the particle size through the restriction of particle growth [16]. The DSC results showed size dependent melting depression behavior and size dependent latent heat of fusion.

Fig. 4 shows the size dependence of the melting points of the synthesized Sn nanoparticle powders, which was compared with Lai et al. model [2]. The solid line was calculated from Eq. (1). Lai et al. obtained this equation based on the model of Hanszen [17] in which it was assumed that the solid particle was embedded in a thin liquid overlayer and the melting temperature was taken to be the temperature of equilibrium between the solid sphere core and the liquid overlayer of a given critical thickness t_0.

$$T_r = 232 - 782\left\{\frac{\sigma_{sl}}{15.8(r - t_0)} - \frac{1}{r}\right\} \qquad (1)$$

where T_r (°C) is the melting points of particles with a radius of r (Å). t_0 (Å) is the critical thickness of the liquid layer. σ_{sl} is the interfacial surface tension between the solid and liquid, the liquid and its vapor. From their experiment, σ_{sl} is determined to be 48 ± 8 mN/m and the best fit for t_0 is 18 Å.

It is found that our experimental results are in reasonable agreement with the Lai et al. model and the melting point depends nonlinearly on the cluster radius.

From Table 1, it could also be found that the latent heat of fusion of the different sized Sn nanoparticles was smaller
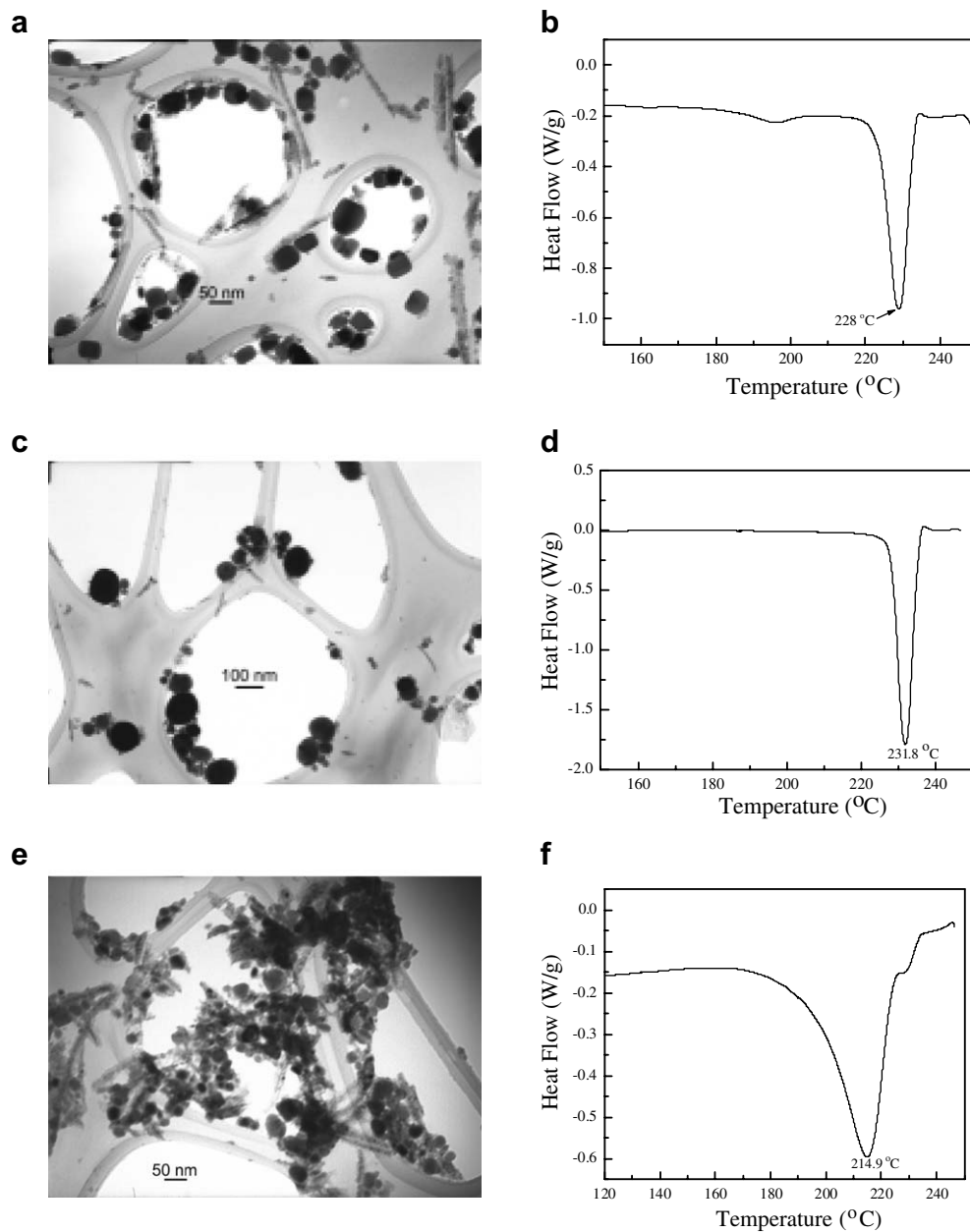
Fig. 3. TEM image and thermal behavior of Sn nanoparticles which were synthesized by using 4.2×10^{-4} mol (a), (b), 1.1×10^{-3} mol (c), (d), 1.75×10^{-4} mol (e), (f) tin (II) acetate as a precursor in the presence of 0.045 mol surfactants.

Table 1
Melting points and heat of fusion of different sized Sn nanoparticles

Samples	Surfactants/precursor	Average size (nm)	Melting point (°C)	ΔH (J/g)
1	N/A	Micron size	232.6	60.0
2	$0.045/1.1 \times 10^{-3}$	85 ± 10	231.8	32.1
3	$0.045/2.1 \times 10^{-4}$	61 ± 10	230.0	24.5
4	$0.045/4.2 \times 10^{-4}$	52 ± 8	228.0	28.7
5	$0.045/1.75 \times 10^{-4}$	26 ± 10	214.9	27.4

than that of micron sized Sn powders. Ercolessi et al. have found that ΔH_m of gold nanoparticles decreases steadily from 114 meV/atom (bulk) to 23 meV/atom ($N = 879$) and 10 meV/atom ($N = 477$) by molecular dynamic simulation [18]. It is also found by experiments that the normalized heat of fusion of Sn nanoparticles decreases markedly from the bulk value (58.9 J/g) by as much as 70% when the particle size is reduced, which can be interpreted as a solid core melting following the gradual surface melting for small particles [2]. We tried to compare the heat of fusion (ΔH_m) of our synthesized Sn particles with Lai et al. model as well [2]. It was found that the ΔH_m values of our Sn particles were smaller than those of their models. This might be due to the existence of the surfactants, solvents and some small amounts of oxides which might develop from the heating process of DSC test.
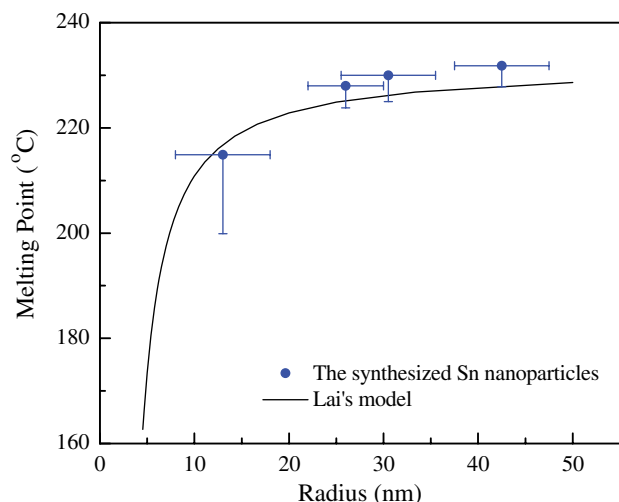
Fig. 4. Size dependence of the melting points of Sn nanoparticles (Y error bars stand for the melting temperature from the onset point to the peak point of DSC curves). The solid line is calculated from Eq. (1) by Lai et al. [2].

4. Conclusions

Sn nanoparticles of various sizes were successfully synthesized via chemical reduction method. Surfactants were used to prevent the synthesized Sn nanoparticles from aggregation and oxidation. The HRTEM and XRD characterizations showed that the as-synthesized Sn nanoparticles were almost at the oxide free status. DSC results showed that different sized Sn nanoparticles had different melting point depression behavior, which matched reasonably with Lai et al. model. The heat of fusion of the as-synthesized Sn nanoparticles was smaller than that of micron sized Sn powders.

Acknowledgement

References

[1] C.R.M. Wronski, Br. J. Appl. Phys. 18 (1967) 1731.
[2] S.L. Lai, J.Y. Guo, V. Petrova, G. Ramanath, L.H. Allen, Phys. Rev. Lett. 77 (1996) 99.
[3] T. Bachels, H.J. Guntherodt, R. Schafer, Phys. Rev. Lett. 85 (2000) 1250.
[4] S.J. Zhao, S.Q. Wang, D.Y. Cheng, H.Q. Ye, J. Phys. Chem. B 105 (2001) 12,857.
[5] A.A. Shvartsburg, M.F. Jarrold, Phys. Rev. Lett. 85 (2000) 2530.
[6] C.L. Cleveland, W.D. Luedtke, U. Landman, Phys. Rev. Lett. 81 (1998) 2036.
[7] M. Schmidt, R. Kusche, B. von Issendorff, H. Haberland, Nature 393 (1998) 238.
[8] L.J. Lewis, P. Jensen, J.L. Barrat, Phys. Rev. B 56 (1997) 2248.
[9] C.L. Cleveland, U. Landman, W.D. Luedtke, J. Phys. Chem. 98 (1994) 6272.
[10] F.G. Shi, J. Mater. Res. 9 (1994) 1307.
[11] Q. Jiang, F.G. Shi, Mater. Lett. 37 (1998) 79.
[12] P. Buffat, J.P. Borel, Phys. Rev. A 13 (1976) 2287.
[13] Y. Kwon, M.G. Kim, Y. Kim, Y. Lee, J. Cho, Electrochem. Solid-State Lett. 9 (2006) A34.
[14] Y. Wang, J.Y. Lee, T.C. Deivaraj, J. Phys. Chem. B 108 (2004) 13,589.
[15] Y. Imry, D. Bergman, Phys. Rev. A 3 (1971) 1416.
[16] M. Mandal, S.K. Ghosh, S. Kundu, K. Esumi, T. Pal, Langmuir 18 (2002) 7792.
[17] K.J. Hanszen, Z. Phys. 157 (1960) 523.
[18] F. Ercolessi, W. Andreoni, E. Tosatti, Phys. Rev. Lett. 66 (1991) 911.